

Line-Node Dirac Semimetal and Topological Insulating Phase in Noncentrosymmetric Pnictides CaAgX ($X = \text{P, As}$)

Ai Yamakage,^{1,3} Youichi Yamakawa,^{2,3} Yukio Tanaka,¹ and Yoshihiko Okamoto^{1,3}

¹*Department of Applied Physics, Nagoya University, Nagoya 464-8603, Japan*

²*Department of Physics, Nagoya University, Nagoya 464-8602, Japan*

³*Institute for Advanced Research, Nagoya University, Nagoya 464-8601, Japan*

Two noncentrosymmetric ternary pnictides, CaAgP and CaAgAs , are reported as topological line-node semimetals protected solely by mirror-reflection symmetry. The band gap vanishes on a circle in momentum space, and surface states emerge within the circle. Extending this study to spin-orbit coupled systems reveals that, compared with CaAgP , a substantial band gap is induced in CaAgAs by large spin-orbit interaction. The resulting states are a topological insulator, in which the \mathbb{Z}_2 topological invariant is given by 1;000. To clarify the \mathbb{Z}_2 topological invariants for time-reversal-invariant systems without spatial-inversion symmetry, we introduce an alternative way to calculate the invariants characterizing a line node and topological insulator for mirror-reflection-invariant systems.

Introduction.— The idea of topology has been greatly expanded in the field of condensed matter physics. The quantum Hall effect can be viewed as a topological insulating state.^{1,2} In the past decade, various topological insulators respecting time-reversal symmetry have been discovered and this has motivated numerous subsequent studies.^{3–5} However, zero-gap semiconductors (Weyl/Dirac semimetals)^{6–9} have recently been recognized as a topologically nontrivial system. The absence of a band gap and the approximately linear dispersion in the low-energy regime are the characteristic features of the Weyl/Dirac semimetals. Because the low-lying excitations are the same as those of relativistic massless fermions, i.e., Weyl/Dirac fermions, anomalous transport phenomena such as the chiral magnetic effect¹⁰ can be expected not only in high-energy physics but also in solids.^{11,12} Thus, exploring topological semimetals can serve as a basis for understanding novel phenomena in condensed matter physics.

In most Weyl/Dirac semimetals, conduction bands overlap with valence bands at certain momentum points. However, the band gap rarely vanishes on a momentum line.^{13–16} Such a dispersion structure is called a “line node,” which is analogous to that in line-node superconductors. Recently, many systems have been proposed as line-node semimetals (e.g., graphite,^{17–19} the heterostructure of topological insulators,²⁰ hyperhoneycomb lattice,²¹ transition-metal monophosphides,²² carbon allotropes,^{23,24} Cu_3N ,²⁵ antiperovskites,²⁶ rare-earth monopnictides,²⁷ and perovskite iridates^{28–31}). Furthermore, several quantum phenomena are also expected to appear in line-node semimetals; these include a flat Landau level,³² long-range Coulomb interaction,³³ the Kondo effect,³⁴ and a quasi-topological electromagnetic response that induces charge polarization and orbital magnetization proportional to the length of the line node.³⁵ Experimental results on line-node semimetal materials are also being reported.^{36–38} Interestingly, in addition to these materials, photonic crystals³⁹ and

spin liquids⁴⁰ have been shown to host line nodes. The line-node structure of energy bands is becoming a prominent topic.

In this Letter, we propose hexagonal pnictides CaAgX ($X = \text{P}$ and As) as novel line-node Dirac semimetals. Mewis synthesized these compounds and found that they crystallize in the ZrNiAl -type structure with space group $\text{P}\bar{6}2\text{m}$.⁴¹ As depicted in Fig. 1(a), AgX_4 tetrahedra form a three-dimensional network by sharing their edges and corners with intervening Ca atoms, which form a kagome-triangular lattice.⁴² An important aspect of this structure in terms of the physics of topology is that the space group has $\text{D}_{3\text{h}}$ point-group symmetry, i.e., mirror-reflection symmetry is preserved while spatial-inversion symmetry is not, although almost all of the previously studied line-node semimetal materials have spatial-inversion symmetry. First-principles calculations and symmetry consideration indicate that there actually exists a line-node in CaAgX . Additionally, the \mathbb{Z}_2 topological invariant regarding a line node is well defined by using mirror-reflection symmetry instead of spatial-inversion symmetry. The relation between the topological invariant and surface states is also discussed. When the spin-orbit interaction is switched on, the line node disappears and the system turns into a topological insulator. We investigate the topological phase of CaAgX both from the energy dispersion on the surface and from the \mathbb{Z}_2 topological invariants, which is obtained to be $\nu_0; \nu_1\nu_2\nu_3 = 1; 000$.

Bulk electronic states.— First, we perform the first-principles calculations by using the WIEN2k code.^{43,44} We use the experimental structural parameters⁴¹ for the calculations. Figure 1(b) shows the calculated band structures of CaAgP without the spin-orbit interaction. The line node is observed within 10 K from the Fermi level along the ΓM and ΓK lines, and it forms a circle in the k_x - k_y plane centered at the Γ point, as illustrated in the inset of Fig. 1(b). The band dispersion at the line node is linear along both the radial and k_z

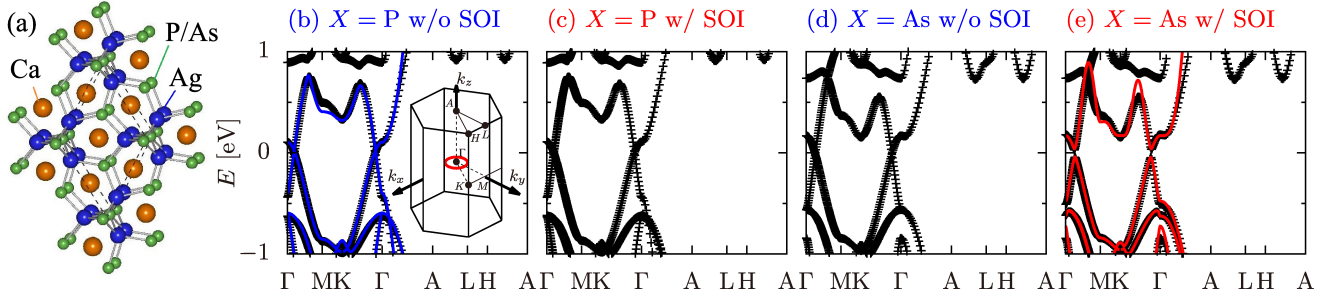


Fig. 1. (a) Crystal structure of CaAgX ($X = \text{P, As}$). Small, middle, and large spheres represent X , Ag , and Ca atoms, respectively. The dotted lines show the hexagonal unit cell. (b)–(e) Electronic states of CaAgP and CaAgAs with (w/) and without (w/o) spin-orbit interaction (SOI). The crosses in (b)–(e) and the solid curves in (b) and (e) indicate the band dispersion obtained by first-principles calculations and by using the tight-binding models, respectively. In the inset of (b), the location of the line node is indicated by the (red) circle around the Γ point in the Brillouin zone.

directions. This line node is not protected for the spin-orbit interaction. However, as shown in Fig. 1(c), the effect of the spin-orbit interaction in CaAgP is negligible and the size of the induced gap at the line node is of the order of 10 K because of the weak spin-orbit interaction in the P atom. In stark contrast, the spin-orbit interaction has a significant effect on the band structures of CaAgAs . We show the calculated band structure of CaAgAs without and with spin-orbit interaction in Figs. 1(d) and 1(e), respectively. The line node has a large gap of ~ 1000 K, indicating that the bulk system is an insulator.

Next, we derive tight-binding models for CaAgP and CaAgAs to investigate the surface electronic states. According to first-principles calculations, the main component of the conduction band at the Γ point is the p_z (A_2'' in D_{3h}) orbital of P or As atoms. In contrast, the valence band around the Γ point mainly consists of the s orbital (A_1' in D_{3h}) of Ag atoms in addition to the p_x and p_y orbitals (E' in D_{3h}) of P or As atoms. Therefore, we construct the 12-orbital tight-binding models by constructing the maximally localized Wannier functions for the $3p$ ($4p$) orbitals of three P (As) atoms and the $5s$ orbital of three Ag atoms in CaAgP (CaAgAs).^{45,46} Furthermore, we have checked that the results do not alter even if the d orbitals of Ca atoms are taken into account.⁴⁷ Here, the spin-orbit interaction $H_{\text{SO}} = \lambda \mathbf{L} \cdot \mathbf{S}$, with $\lambda = 0.07$ eV for $4p$ electrons, is taken into account in the CaAgAs model, whereas it is neglected in the CaAgP model. In Figs. 1(b) and 1(e), we see a good agreement between the first principle band and the obtained tight-binding band.

Topological line node and surface states in CaAgP .— Figure 2(a) shows the angle-resolved density of states, calculated from the surface Green's function via the QZ decomposition,^{48,49} on the (0001) surface terminated at a Ca_3P layer. Note that two types of termination, Ca_3X and Ag_3X_2 , are possible on the (0001) surface of CaAgX . Hereafter, we focus only on the former type of termination.⁵⁰ One can clearly see that a line node is located around the $\bar{\Gamma}$ point, which is projected from the bulk line node, and there exist surface states within the node.

The bulk line node is protected by mirror-reflection sym-

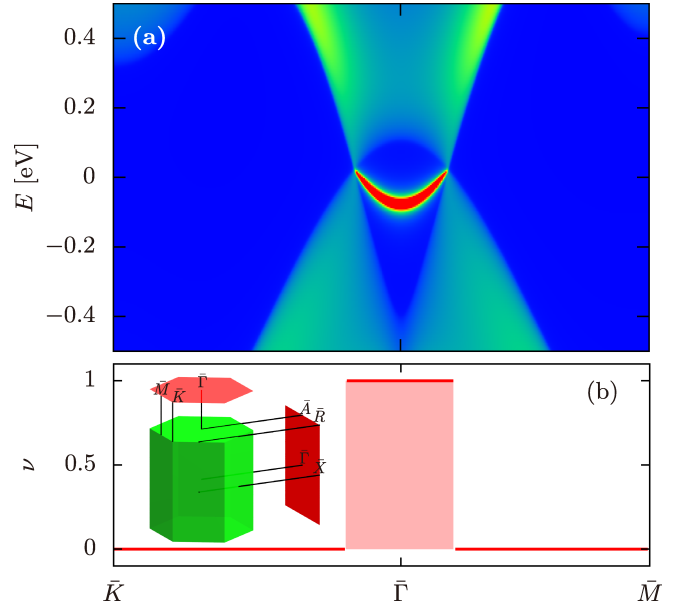


Fig. 2. Angle-resolved density of states on the (0001) surface with the Ca_3P termination (a) and the topological number ν of CaAgP (b). The inset in (b) shows the projected Brillouin zones onto the (0001) and $(10\bar{1}0)$ surfaces.

metry with respect to the horizontal plane: $H(k_x, k_y, k_z) = M^\dagger H(k_x, k_y, -k_z)M$. The conduction and valence bands belong to A_2'' and A_1' representations, respectively; therefore, these bands are degenerate on the mirror-reflection invariant plane of $k_z = 0$. Mirror-reflection symmetry allows one to introduce the \mathbb{Z}_2 topological invariant ν to characterize the band inversion as

$$(-1)^{\nu(k_x, k_y)} = \xi(k_x, k_y, 0)\xi(k_x, k_y, \pi). \quad (1)$$

Here, $\xi(\mathbf{k})$ is the product of eigenvalues of the mirror reflection for all the occupied bands at \mathbf{k} . Obviously, $\nu(k_x, k_y) = 1$ indicates band inversion from $k_z = 0$ to $k_z = \pi$. Moreover, it is worth mentioning that $\nu(k_x, k_y)$ is related to the Berry phase:⁵¹

$$(-1)^{\nu(k_x, k_y)} = \exp \left[i \int_{-\pi}^{\pi} dk_z \text{tr} A_z(\mathbf{k}) + \text{tr} \ln B(k_x, k_y) \right], \quad (2)$$

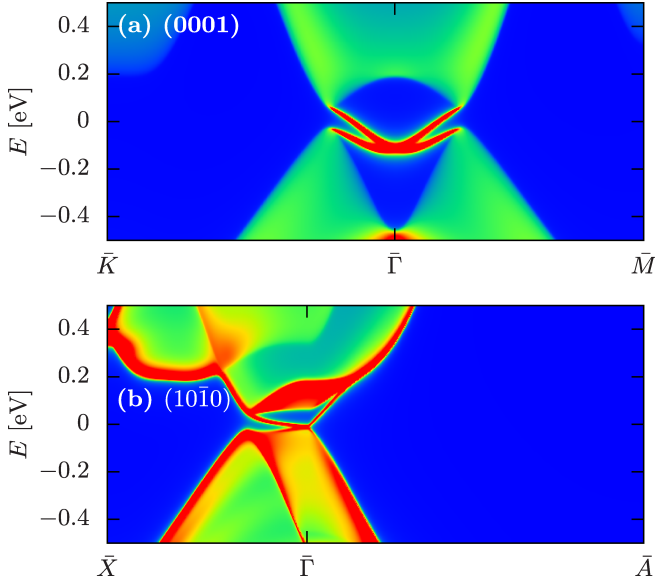


Fig. 3. Angle-resolved density of states on the (a) Ca_3As -terminated (0001) and (b) $(10\bar{1}0)$ surfaces of CaAgAs .

where the non-Abelian Berry connection is defined by

$$[A(\mathbf{k})]_{mn} = -i\langle \mathbf{k}, m | \frac{\partial}{\partial \mathbf{k}} | \mathbf{k}, n \rangle, \quad (3)$$

where $|\mathbf{k}, m\rangle$ denotes an occupied eigenstate. $B(k_x, k_y)$ is the sewing matrix defined by

$$[B(k_x, k_y)]_{mn} = \langle (k_x, k_y, \pi), m | B_z | (k_x, k_y, \pi) - \mathbf{G}_z, n \rangle, \quad (4)$$

where B_j is an operator satisfying

$$H(\mathbf{k}) = B_j^\dagger H(\mathbf{k} + \mathbf{G}_j) B_j, \quad (5)$$

and $\mathbf{G}_j = 2\pi\hat{x}_j$ denotes the j -th reciprocal lattice vector. The calculated $\nu(k_x, k_y)$ is shown in Fig. 2(b). The topological invariant is obtained to be nontrivial, $\nu(k_x, k_y) = 1$, within the line node, while trivial, $\nu(k_x, k_y) = 0$, in the outside. Since $\nu(k_x, k_y)$ is invariant for a continuous change of parameters of the Hamiltonian, the line node is a topologically stable object.

Topological insulating phase in CaAgAs .— The degeneracy in dihedral point-group symmetry is lifted by the spin-orbit interaction. Correspondingly, the product of the eigenvalues of mirror reflection is always unity: $\xi(k_x, k_y, 0)\xi(k_x, k_y, \pi) = 1$; namely, the \mathbb{Z}_2 invariant takes the trivial value $\nu(k_x, k_y) = 0$.⁵² This means that the spin-orbit interaction yields an energy gap in the line node. Furthermore, the spin-orbit interaction gives rise to a transition from a line-node semimetal to a topological insulator. Figure 3 shows the angle-resolved density of states on the (0001) and $(10\bar{1}0)$ surfaces. In the spin-orbit gap (~ 0.1 eV), gapless surface states appear. The Dirac point is located at the $\bar{\Gamma}$ point. On the (0001) surface [Fig. 3(a)], the gapless surface states are smoothly deformed from those in the absence of spin-orbit interaction [Fig. 2(a)]. On the $(10\bar{1}0)$ surface, gapless surface states with approximately linear dispersion emerge in the induced band

Table I. Berry phase $\Phi_{jli\eta}(k_l)$ and \mathbb{Z}_2 invariant $\nu_{li\eta}$ of CaAgAs .

i	1	1	2	2	3	3
η	0	1	0	1	0	1
$\Phi_{jli\eta}(k_l = 0)$	2π	0	2π	0	2π	0
$\Phi_{jli\eta}(k_l = \pi)$	0	0	0	0	0	0
$\nu_{li\eta}$	1	0	1	0	1	0

gap. The in-plane ($\bar{\Gamma}\bar{X}$) velocity of the surface Dirac fermion is slower than the out-of-plane ($\bar{\Gamma}\bar{A}$) one, since the lattice constant along the c axis is so small ($c/a \sim 0.6$) that the interlayer coupling is much stronger.

The obtained gapless surface states, shown in Fig. 3, coincide with the \mathbb{Z}_2 topological invariants of $\nu_0; \nu_1\nu_2\nu_3 = 1; 000$. The simplified formula for the invariant derived by Fu and Kane⁵³ cannot be applied to the present system owing to the lack of spatial-inversion symmetry. Instead, with the help of mirror-reflection symmetries with respect to the horizontal $H(k_x, k_y, k_z) = M_z^\dagger H(k_x, k_y, k_z) M_z$ and the vertical $H(k_x, k_y, k_z) = M_y^\dagger H(k_x, -k_y, k_z) M_y$ planes, the topological invariants can be easily calculated as

$$\nu_{li\eta} = \frac{\Phi_{jli\eta}(k_l = 0) + \Phi_{jli\eta}(k_l = \pi)}{2\pi} \pmod{2}, \quad (6)$$

for $i, j, l = 1, 2, 3$ ($i \neq j \neq l \neq i$) and $\eta = 0, 1$.⁵⁴ The \mathbb{Z}_2 topological invariants are obtained by $\nu_0 = \nu_{i0} + \nu_{i1} \pmod{2}$, $\nu_i = \nu_{i1}$. The Berry phase is given by

$$\Phi_{jli\eta}(k_l) = \int_{-\pi}^{\pi} dk_j \text{tr} A_j(\mathbf{k})|_{k_j=\eta\pi} - i \text{tr} \ln B_{jli\eta}(k_l), \quad (7)$$

where $B_{jli\eta}(k_l)$ is the sewing matrix defined by

$$[B_{jli\eta}(k_l)]_{mn} = \langle \mathbf{k}, m | B_j | \mathbf{k} - \mathbf{G}_j, n \rangle|_{k_j=\pi, k_l=\eta\pi}. \quad (8)$$

Formula (7) is useful because only two points $k_l = 0$ and $k_l = \pi$ are needed for the calculation, as in the case of spatial-inversion invariant systems.³⁰ The calculated Berry phases are summarized in Table I. All the Berry phases on the zone boundaries $k_l = \pi$ are zero, resulting in the topological invariants of 1; 000.⁵⁵

Effective model.— We now derive effective models for CaAgP and CaAgAs . In the model of CaAgAs (CaAgP), we (do not) take into account the spin-orbit interaction.

As discussed above, the conduction and valence bands at the Γ point of CaAgP mainly consist of the A_2'' and A_1' states, respectively. Thus, the low-energy electronic structure is effectively described by the two-band model

$$H_{\text{CaAgP}}(\mathbf{k}) = c(\mathbf{k}) + m(\mathbf{k})\sigma_z + vk_z\sigma_y, \quad (9)$$

with $c(\mathbf{k}) = c_0 + c_1k_z^2 + c_2(k_x^2 + k_y^2)$ and $m(\mathbf{k}) = m_0 + m_1k_z^2 + m_2(k_x^2 + k_y^2)$ in the vicinity of the Γ point. A line node appears on the $k_z = 0$ plane under the band-inversion condition of $m_0m_2 < 0$.

In CaAgAs , the four-fold degenerated valence-band states at the Γ point without the spin-orbit interaction, which consist of E' states, are split into two doublets ($E_{3/2}$ and $E_{5/2}$) by in-

roducing the spin-orbit interaction. The resulting low-energy states consist of the $E_{5/2}$ doublet in the valence band and the $E_{3/2}$ doublet in the conduction band, which are described by the Hamiltonian

$$H_{\text{CaAgAs}}(\mathbf{k}) = \begin{pmatrix} h(\mathbf{k}) & \Lambda(\mathbf{k}) \\ \Lambda(\mathbf{k})^\dagger & h(-\mathbf{k})^* \end{pmatrix}. \quad (10)$$

$h(\mathbf{k})$ is the 2×2 Hamiltonian matrix for the states in which the z components of the total angular momentum are given by $j_z = 1/2$ and by $j_z = 3/2$. $h(\mathbf{k})$ reads

$$h(\mathbf{k}) = c(\mathbf{k}) + m(\mathbf{k})\sigma_z + Ak_z(k_x\sigma_x - k_y\sigma_y), \quad (11)$$

up to the second order of k . $\Lambda(\mathbf{k})$ is the 2×2 matrix representing the spin-mixing effect induced by the spin-orbit interaction, defined by $\Lambda(\mathbf{k}) = \Lambda_1(\mathbf{k}) + \Lambda_2(\mathbf{k})$, where

$$\Lambda_1(\mathbf{k}) = -iB_\perp k_z(1 - \sigma_z) + -iB_\parallel(k_x + ik_y)\sigma_x, \quad (12)$$

$$\Lambda_2(\mathbf{k}) = D\sigma_y \left[-i(k_x^2 - k_y^2) - 2k_x k_y \right]. \quad (13)$$

$\Lambda(\mathbf{k})$ yields a finite energy gap on the $k_z = 0$ plane, thereby turning the system into a strong topological insulator with 1;000.

These two effective Hamiltonians qualitatively describe the electronic structures of CaAgP and CaAgAs. Therefore, it is useful for a further analysis of the electromagnetic responses and transport properties of these materials. These Hamiltonians, however, do not quantitatively reproduce the low-energy electronic states, because the line node is located rather far from the Γ point. To obtain a quantitatively good model, one has to take into account higher energy states in addition to the low-lying states.

Summary.— We have clarified the topological electronic structure of hexagonal pnictides CaAgX ($X = \text{P}$ and As). CaAgX is a line-node Dirac semimetal in the absence of spin-orbit interaction. In reality, CaAgP exhibits line-node-semimetal properties except in the very low energy and low-temperature regime owing to the tiny spin-orbit interaction (~ 10 K). When P atoms are replaced with heavier As atoms, the strong spin-orbit interaction widens the size of the band gap considerably at the line node. CaAgAs is found to be a strong topological insulator with the \mathbb{Z}_2 invariant of 1;000.

It has been known that the presence of reflection symmetry and band inversion is necessary and sufficient for the existence of a line node, whereas most of the line-node Dirac semimetals proposed so far preserve spatial-inversion symmetry. Moreover, the \mathbb{Z}_2 topological invariant characterizing the line node was defined in previous works in terms of PT symmetry.^{15,25} This invariant cannot be directly applied to systems lacking inversion symmetry, including CaAgX reported here. We have introduced the alternative \mathbb{Z}_2 invariant $\nu(k_x, k_y)$ in this study, which is applicable to systems without spatial-inversion symmetry. This implies that line-node Dirac semimetals with and without spatial-inversion symmetry might exhibit intrinsically different electromagnetic responses and transport phenomena, which are related to the topological invariants. Superconductivity of line-node

semimetals is another interesting topic, as discussed in point-node Weyl^{56–61} and Dirac semimetals.⁶² These issues will be addressed in future works.

Note added.— After the submission of this paper, we became aware of a recent preprint⁶³ in which the relation between the Berry phase and eigenvalues of mirror reflection is discussed in a form different from Eqs. (1) and (2).

Acknowledgment The authors are grateful to S. Kobayashi for valuable discussion.

- 1) D. J. Thouless, M. Kohmoto, M. P. Nightingale, and M. den Nijs: Phys. Rev. Lett. **49** (1982) 405.
- 2) M. Kohmoto: Ann. Phys. **160** (1985) 343 .
- 3) M. Z. Hasan and C. L. Kane: Rev. Mod. Phys. **82** (2010) 3045.
- 4) X.-L. Qi and S.-C. Zhang: Rev. Mod. Phys. **83** (2011) 1057.
- 5) Y. Tanaka, M. Sato, and N. Nagaosa: J. Phys. Soc. Jpn. **81** (2012) 011013.
- 6) S. Murakami: New J. Phys. **9** (2007) 356.
- 7) X. Wan, A. M. Turner, A. Vishwanath, and S. Y. Savrasov: Phys. Rev. B **83** (2011) 205101.
- 8) S. M. Young, S. Zaheer, J. C. Y. Teo, C. L. Kane, E. J. Mele, and A. M. Rappe: Phys. Rev. Lett. **108** (2012) 140405.
- 9) J. A. Steinberg, S. M. Young, S. Zaheer, C. L. Kane, E. J. Mele, and A. M. Rappe: Phys. Rev. Lett. **112** (2014) 036403.
- 10) K. Fukushima, D. E. Kharzeev, and H. J. Warringa: Phys. Rev. D **78** (2008) 074033.
- 11) A. A. Zyuzin, S. Wu, and A. A. Burkov: Phys. Rev. B **85** (2012) 165110.
- 12) P. Hosur and X. Qi: Compt. Rend. Phys. **14** (2013) 857.
- 13) A. A. Burkov, M. D. Hook, and L. Balents: Phys. Rev. B **84** (2011) 235126.
- 14) C.-K. Chiu and A. P. Schnyder: Phys. Rev. B **90** (2014) 205136.
- 15) C. Fang, Y. Chen, H.-Y. Kee, and L. Fu: Phys. Rev. B **92** (2015) 081201.
- 16) Z. Gao, M. Hua, H. Zhang, and X. Zhang: arXiv:1507.07504 .
- 17) G. P. Mikitik and Y. V. Sharlai: Phys. Rev. B **73** (2006) 235112.
- 18) T. T. Heikkilä and G. E. Volovik: JETP Lett. **93** (2011) 59.
- 19) T. T. Heikkilä and G. E. Volovik: arXiv:1505.03277 .
- 20) M. Phillips and V. Aji: Phys. Rev. B **90** (2014) 115111.
- 21) K. Mullen, B. Uchoa, and D. T. Glatzhofer: Phys. Rev. Lett. **115** (2015) 026403.
- 22) H. Weng, C. Fang, Z. Fang, B. A. Bernevig, and X. Dai: Phys. Rev. X **5** (2015) 011029.
- 23) H. Weng, Y. Liang, Q. Xu, R. Yu, Z. Fang, X. Dai, and Y. Kawazoe: Phys. Rev. B **92** (2015) 045108.
- 24) Y. Chen, Y. Xie, S. A. Yang, H. Pan, F. Zhang, M. L. Cohen, and S. Zhang: arXiv:1505.02284 .
- 25) Y. Kim, B. J. Wieder, C. L. Kane, and A. M. Rappe: Phys. Rev. Lett. **115** (2015) 036806.
- 26) R. Yu, H. Weng, Z. Fang, X. Dai, and X. Hu: Phys. Rev. Lett. **115** (2015) 036807.
- 27) M. Zeng, C. Fang, G. Chang, Y.-A. Chen, T. Hsieh, A. Bansil, H. Lin, and L. Fu: arXiv:1504.03492 .
- 28) J.-M. Carter, V. V. Shankar, M. A. Zeb, and H.-Y. Kee: Phys. Rev. B **85** (2012) 115105.
- 29) Y. Chen, Y.-M. Lu, and H.-Y. Kee: Nature Communications **6** (2015) 6593.
- 30) H.-S. Kim, Y. Chen, and H.-Y. Kee: Phys. Rev. B **91** (2015) 235103.
- 31) J. Liu, D. Krieger, L. Horak, D. Puggioni, C. Rayan Serrao, R. Chen, D. Yi, C. Frontera, V. Holy, A. Vishwanath, J. M. Rondinelli, X. Marti, and R. Ramesh: arXiv:1506.03559 .
- 32) J.-W. Rhim and Y. B. Kim: Phys. Rev. B **92** (2015) 045126.
- 33) Y. Huh, E.-G. Moon, and Y. B. Kim: arXiv:1506.05105 .
- 34) A. K. Mitchell and L. Fritz: arXiv:1506.05491 .
- 35) S. T. Ramamurthy and T. L. Hughes: arXiv:1508.01205 .

- 36) L. S. Xie, L. M. Schoop, E. M. Seibel, Q. D. Gibson, W. Xie, and R. J. Cava: *APL Mater.* **3** (2015) 083602.
- 37) G. Bian, T.-R. Chang, R. Sankar, S.-Y. Xu, H. Zheng, T. Neupert, C.-K. Chiu, S.-M. Huang, G. Chang, I. Belopolski, D. S. Sanchez, M. Neupane, N. Alidoust, C. Liu, B. Wang, C.-C. Lee, H.-T. Jeng, A. Bansil, F. Chou, H. Lin, and M. Zahid Hasan: arXiv:1505.03069 .
- 38) L. M. Schoop, M. N. Ali, C. Straßer, V. Duppe, S. S. P. Parkin, B. V. Lotsch, and C. R. Ast: arXiv:1509.00861 .
- 39) L. Lu, L. Fu, J. D. Joannopoulos, and M. Soljačić: *Nat. Photo.* **7** (2013) 294.
- 40) W. M. H. Natori, E. Miranda, and R. G. Pereira: arXiv:1505.06171 .
- 41) A. Mewis: *Zeitschrift für Naturforschung B* **34** (1979) 14.
- 42) H. Ishikawa, T. Okubo, Y. Okamoto, and Z. Hiroi: *J. Phys. Soc. Jpn.* **83** (2014) 043703.
- 43) P. Blaha, K. Schwarz, G. Madsen, D. Kvasnicka, and J. Luitz: *WIEN2k, An Augmented Plane Wave + Local Orbitals Program for Calculating Crystal Properties* (Techn. Universität Wien, Austria, 2001).
- 44) We used the full-potential linearized augmented plane-wave method within the generalized gradient approximation as implemented in the WIEN2k code.⁴³ $24 \times 24 \times 36$ k -points sampling was used for the self-consistent calculation.
- 45) N. Marzari and D. Vanderbilt: *Phys. Rev. B* **56** (1997) 12847.
- 46) I. Souza, N. Marzari, and D. Vanderbilt: *Phys. Rev. B* **65** (2001) 035109.
- 47) See Sec. S 4 of Supplemental Material.
- 48) T. Miyata, S. Honda, R. Naito, and S.-L. Zhang: *Jpn. J. Ind. Appl. Math.* **30** (2013) 653.
- 49) T. Miyata, R. Naito, and S. Honda: *J. Eng. Math.* (2015) 1.
- 50) Electronic states on the Ag_3X_2 termination is shown in Sec. S 1 of Supplemental Material.
- 51) Equation (1) is derived from Eq. (2). See Sec. S 2 of Supplemental Material.
- 52) See Sec. S 2.4 of Supplemental Material.
- 53) L. Fu and C. L. Kane: *Phys. Rev. B* **76** (2007) 045302.
- 54) Equation (6) is obtained for mirror-reflection-invariant systems. See Sec. S 3 of Supplemental Material.
- 55) Dirac semimetals in which a line node is located around the Γ point always becomes a strong topological insulator with $\nu_0; \nu_1 \nu_2 \nu_3 = 1; 000$ when spin-orbit interaction is switched on. See Sec. S 3.3 of Supplemental Material.
- 56) G. Y. Cho, J. H. Bardarson, Y.-M. Lu, and J. E. Moore: *Phys. Rev. B* **86** (2012) 214514.
- 57) V. Shivamoggi and M. J. Gilbert: *Phys. Rev. B* **88** (2013) 134504.
- 58) H. Wei, S.-P. Chao, and V. Aji: *Phys. Rev. B* **89** (2014) 014506.
- 59) H. Wei, S.-P. Chao, and V. Aji: *Phys. Rev. B* **89** (2014) 235109.
- 60) B. Lu, K. Yada, M. Sato, and Y. Tanaka: *Phys. Rev. Lett.* **114** (2015) 096804.
- 61) G. Bednik, A. A. Zyuzin, and A. A. Burkov: *Phys. Rev. B* **92** (2015) 035153.
- 62) S. Kobayashi and M. Sato: arXiv:1504.07408 .
- 63) Y.-H. Chan, C.-K. Chiu, M. Y. Chou, and A. P. Schnyder: arXiv:1510.02759 .
- 64) S. Kobayashi *et al.*, in preparation.
- 65) R. Yu, X. L. Qi, A. Bernevig, Z. Fang, and X. Dai: *Phys. Rev. B* **84** (2011) 075119.
- 66) L. Fu and E. Berg: *Phys. Rev. Lett.* **105** (2010) 097001.
- 67) X.-L. Qi, T. L. Hughes, and S.-C. Zhang: *Phys. Rev. B* **81** (2010) 134508.
- 68) M. Sato: *Phys. Rev. B* **81** (2010) 220504.

S 1. Termination-dependent (0001) surface states

CaAgX consists of alternating stacking of Ca_3X and Ag_3X_2 layers along the c axis, i.e., the (0001) surface can be terminated by either of these layers. Correspondingly, energy dispersion relations of (0001) surface states on the Ca_3X termination are different from those on the Ag_3X_2 termination.

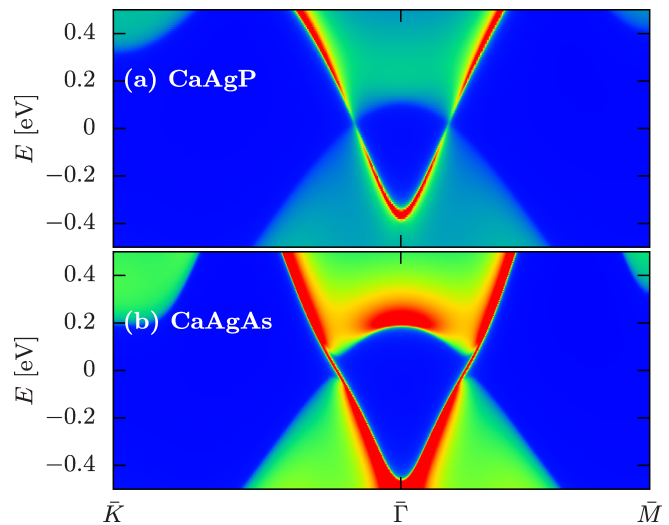


Fig. S 1. Angle-resolved density of states on the (0001) surface with the Ag_3X_2 termination for $X = \text{P}$ (a), As (b).

Angle-resolve density of states on the Ag_3X_2 termination is shown in Fig. S 1. Surface states on the Ca_3X termination of CaAgP (CaAgAs) show up within the (gapped) line node, as shown in Fig. 2(a) [3(a)], while those on the Ag_3X_2 termination do not, as shown in Fig. S 1.

S 2. \mathbb{Z}_2 line node protected by mirror-reflection symmetry

A line node protected by mirror-reflection symmetry is simply understood as follows: conduction and valence bands have opposite parity of the reflection hence these are degenerated at the reflection invariant plane $k_z = 0$ or $k_z = \pi$. Here, we show that the topological invariant which is associated with a line node can be defined in terms of Berry phase.

S 2.1 Definition

Suppose a system preserving mirror-reflection symmetry with respect to the horizontal plane. The Hamiltonian $H(\mathbf{k})$ satisfies

$$H(k_x, k_y, k_z) = M^\dagger H(k_x, k_y, -k_z)M. \quad (\text{S14})$$

Mirror-reflection operator M , in general, depends on k_z in systems with sublattice structure. In the following, we choose the gauge in which M is independent of k_z . Instead, the Hamiltonian has a nontrivial periodicity:

$$H(\mathbf{k}) = B^\dagger H(\mathbf{k} + \mathbf{G}_z)B, \quad (\text{S15})$$

where $\mathbf{G}_z = (0, 0, 2\pi)$ denotes the reciprocal lattice vector along the z axis. The \mathbb{Z}_2 topological invariant $\nu(k_x, k_y)$ is defined by

$$(-1)^{\nu(k_x, k_y)} = \exp \left[i \int_{-\pi}^{\pi} dk_z \text{tr} A_z(\mathbf{k}) + \text{tr} \ln B(k_x, k_y) \right]. \quad (\text{S16})$$

The non-Abelian Berry connection $A(\mathbf{k})$ and unitary matrix $B(k_x, k_y)$ are defined by

$$[A(\mathbf{k})]_{mn} = -i\langle \mathbf{k}, m | \frac{\partial}{\partial \mathbf{k}} | \mathbf{k}, n \rangle, \quad (\text{S17})$$

and

$$[B(k_x, k_y)]_{mn} = \langle (k_x, k_y, \pi), m | B | (k_x, k_y, -\pi), n \rangle. \quad (\text{S18})$$

S 2.2 Gauge symmetry

Next, we show that $\nu(k_x, k_y) \bmod 2$ is invariant under a $U(N)$ gauge transformation $|\mathbf{k}, m\rangle \rightarrow |\mathbf{k}, n\rangle [g(\mathbf{k})]_{nm}$, $g(\mathbf{k}) \in U(N)$. $A(\mathbf{k})$ and $B(k_x, k_y)$ are transformed into

$$A(\mathbf{k}) \rightarrow g^\dagger(\mathbf{k}) A(\mathbf{k}) g(\mathbf{k}) - i g^\dagger(\mathbf{k}) \frac{\partial g(\mathbf{k})}{\partial \mathbf{k}}, \quad (\text{S19})$$

$$B(k_x, k_y) \rightarrow g^\dagger(k_x, k_y, \pi) B(k_x, k_y) g(k_x, k_y, -\pi). \quad (\text{S20})$$

From the integral

$$\int_{-\pi}^{\pi} dk_z \text{tr} g^\dagger(\mathbf{k}) \frac{\partial g(\mathbf{k})}{\partial k_z} = \ln \frac{\det g(k_x, k_y, \pi)}{\det g(k_x, k_y, -\pi)} + i2n\pi, \quad n \in \mathbb{Z}, \quad (\text{S21})$$

one can verify that the right hand side of Eq. (S16) is invariant under the gauge transformation.

S 2.3 \mathbb{Z}_2 invariant and mirror-reflection symmetry

If the system has mirror-reflection symmetry, $\nu(k_x, k_y)$ is the \mathbb{Z}_2 invariant. The mirror-reflection symmetry requires the following relation;

$$H(k_x, k_y, k_z) = M^\dagger H(k_x, k_y, -k_z) M. \quad (\text{S22})$$

We introduce the unitary matrix $M(\mathbf{k})$ in the occupied subspace;

$$[M(k_x, k_y, k_z)]_{mn} = \langle (k_x, k_y, k_z), m | M | (k_x, k_y, -k_z), n \rangle. \quad (\text{S23})$$

On the reflection invariant plane of $k_z = 0$, the states are simultaneously the eigenstates of M hence

$$\det M(k_x, k_y, 0) = \pm 1, \quad (\text{S24})$$

where the phase of M is fixed as $M^2 = 1$. On the other reflection invariant plane of $k_z = \pi$, the mirror-reflection operator is modified to

$$M' = M B^\dagger. \quad (\text{S25})$$

M' satisfies

$$[H(k_x, k_y, \pi), M'] = 0. \quad (\text{S26})$$

Unitary matrix defined by

$$[M'(k_x, k_y, \pi)]_{mn} = \langle (k_x, k_y, \pi), m | M' | (k_x, k_y, \pi), n \rangle, \quad (\text{S27})$$

also satisfies

$$\det M'(k_x, k_y, \pi) = \pm 1. \quad (\text{S28})$$

Now we prove that $\nu(k_x, k_y)$ is the \mathbb{Z}_2 invariant. The non-

Abelian Berry connection satisfies

$$A_z(k_x, k_y, k_z) = -M^\dagger(k_x, k_y, -k_z) A_z(k_x, k_y, -k_z) M(k_x, k_y, -k_z) + i M^\dagger(k_x, k_y, -k_z) \frac{\partial M(k_x, k_y, -k_z)}{-\partial k_z}. \quad (\text{S29})$$

Therefore, the integral of A reduces to

$$\int_{-\pi}^0 dk_z \text{tr} A_z(\mathbf{k}) = - \int_0^\pi dk_z \text{tr} A_z(\mathbf{k}) + i \int_0^\pi dk_z \text{tr} M^\dagger(\mathbf{k}) \frac{\partial M(\mathbf{k})}{\partial k_z}. \quad (\text{S30})$$

The second term is rewritten as

$$i \int_0^\pi dk_z \text{tr} M^\dagger(\mathbf{k}) \frac{\partial M(\mathbf{k})}{\partial k_z} = i \ln \frac{\det M(k_x, k_y, \pi)}{\det M(k_x, k_y, 0)} + 2n\pi. \quad (\text{S31})$$

Consequently, one obtains

$$i \int_{-\pi}^{\pi} dk_z \text{tr} A_z(\mathbf{k}) + \text{tr} \ln B(k_x, k_y) = - \ln \frac{\det M'(k_x, k_y, \pi)}{\det M(k_x, k_y, 0)} + i2n\pi, \quad (\text{S32})$$

namely

$$(-1)^{\nu(k_x, k_y)} = \frac{\det M'(k_x, k_y, \pi)}{\det M(k_x, k_y, 0)} = \pm 1, \quad (\text{S33})$$

which is the same as Eq. (1) in the main manuscript.

S 2.4 Topological invariant in spinful systems

In spinful systems, the topological invariants of spin up and down may cancel each other out; $\nu(k_x, k_y) = 0$, owing to time-reversal T symmetry. The mirror reflection in spinful systems involves the spin hence $T^{-1} M T = -M$, and

$$M(\mathbf{k})^* = -T(-\mathbf{k})^\dagger M(-\mathbf{k}) T(-\mathbf{k}), \quad (\text{S34})$$

where unitary skew matrix $T(\mathbf{k})$ is defined by

$$[T(\mathbf{k})]_{mn} = \langle \mathbf{k}, m | T | -\mathbf{k}, n \rangle. \quad (\text{S35})$$

As a result, one obtains

$$\text{tr} M(k_x, k_y, 0) = -\text{tr} M(-k_x, -k_y, 0), \quad (\text{S36})$$

$$\text{tr} M'(k_x, k_y, \pi) = -\text{tr} M'(-k_x, -k_y, \pi). \quad (\text{S37})$$

For (k_x, k_y, Γ) , $\Gamma = 0, \pi$, which is continuously connected (without gap closing) to a time-reversal invariant momentum Γ within the $k_z = \Gamma$ plane, the following relation holds

$$\text{tr} M(k_x, k_y, 0) = \text{tr} M'(k_x, k_y, \pi) = 0, \quad (\text{S38})$$

since $\text{tr} M(\Gamma) = \text{tr} M'(\Gamma) = 0$ and $\text{tr} M(k_x, k_y, \Gamma)$ is a quantized invariant. Consequently, the number of occupied states with the eigenvalue of $+i$ of mirror reflection are the same as that with the eigenvalue of $-i$. This proves that $\det M(k_x, k_y, 0) = \det M(k_x, k_y, \pi) = (-1)^{N/2}$, $\nu(k_x, k_y) = 0$, where N denotes the number of occupied bands, and that there is no line node encircling time-reversal invariant momenta. Note that line nodes not around time-reversal invariant momenta may appear in a case that antisymmetric spin-orbit interaction is much stronger than symmetric one,⁶⁴ nevertheless it is not the case in an actual material CaAgX.

S 3. \mathbb{Z}_2 invariant and mirror-reflection symmetry in the presence of spin-orbit interaction

We show that the \mathbb{Z}_2 invariant characterizing insulators which respect both time-reversal and mirror-reflection symmetries reduces to the one-dimensional topological invariant Eq. (1).

S 3.1 Definition

We start with the following expression

$$\nu = \int_0^\pi \frac{dk_y}{2\pi} \frac{\partial \Phi(k_y)}{\partial k_y} - \frac{\Phi(\pi) - \Phi(0)}{2\pi} \pmod{2}. \quad (\text{S39})$$

$\Phi(k_y)$ is the Berry phase defined by

$$\Phi(k_y) = \int_{-\pi}^\pi dk_x \text{tr} A_x(\mathbf{k}) - i \text{tr} \ln B(k_y), \quad (\text{S40})$$

with

$$[B(k_y)]_{mn} = \langle (\pi, k_y), m | B | (-\pi, k_y), n \rangle. \quad (\text{S41})$$

Operator B satisfies

$$H(k_x, k_y) = B^\dagger H(k_x + 2\pi, k_y) B. \quad (\text{S42})$$

Equations (S39) and (S40) are equivalent to the \mathbb{Z}_2 invariant derived in Ref.⁶⁵ This is obviously confirmed in a particular choice of gauge in which B is the identity.

S 3.2 Mirror-reflection symmetry and reduced formula

Now we prove

$$\nu = \frac{\Phi(0) + \Phi(\pi)}{2\pi} \pmod{2}, \quad (\text{S43})$$

in the presence of mirror-reflection symmetry as

$$H(k_x, k_y) = M^\dagger H(-k_x, k_y) M. \quad (\text{S44})$$

In a manner similar to Secs. S 2.3 and S 2.4, $\Phi(k_y)$ reduces to

$$\Phi(k_y) = 2n\pi, \quad n \in \mathbb{Z}. \quad (\text{S45})$$

$\Phi(k_y) \pmod{2\pi}$ for $k_y \neq 0, \pi$ is gauge invariant, while on the time-reversal invariant momenta $\Phi(0) \pmod{4\pi}$ and $\Phi(\pi) \pmod{4\pi}$ are.⁶⁵ This means that only $\Phi(0)$ and $\Phi(\pi)$ determines the \mathbb{Z}_2 invariant. Then we arrive at Eq. (S43).

S 3.3 Line node and strong topological insulator

Suppose a system hosting a line node located on the $k_z = 0$ plane around the Γ point in the Brillouin zone, as in the case of CaAgX discussed in the main manuscript. Spin-orbit interaction induces an energy gap at the line node. Here we calculate the \mathbb{Z}_2 topological invariant. On the $k_x = 0$ and $k_x = \pi$ planes, the invariant is given by

$$\nu_{1\eta} = \frac{\Phi_{321\eta}(0) + \Phi_{321\eta}(\pi)}{2\pi} \pmod{2}, \quad (\text{S46})$$

where the subscript is defined in Eq. (7). Berry phase $\Phi_{321\eta}(\Gamma)$ is given by the integral along the k_z axis on the zone center and zone boundary, where the energy gap does not vanish as one turns off the spin-orbit interaction. From this fact, the Berry

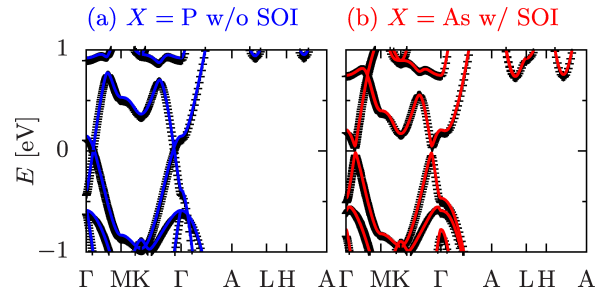


Fig. S 2. Bulk electronic states of (a) CaAgP without spin-orbit interaction and (b) CaAgAs with spin-orbit interaction. Energy bands obtained by using the 27-orbital tight-binding model and by first-principles calculation are denoted by the solid lines and by the crosses, respectively.

phase reduces to that in the absence of spin-orbit interaction;

$$\Phi_{321\eta}(\Gamma) = \Phi_{321\eta}^\uparrow(\Gamma) + \Phi_{321\eta}^\downarrow(\Gamma) = 2\Phi_{321\eta}^\uparrow(\Gamma), \quad (\text{S47})$$

where Φ^\uparrow and Φ^\downarrow denote the Berry phase in the spin-up and spin-down subspaces without spin-orbit interaction. A similar technique is found in Refs.^{66–68} Furthermore, from Eqs. (S32) and (S33),

$$\Phi_{321\eta}(\Gamma) = 2\pi\nu(\eta\pi, \Gamma) \pmod{4\pi}. \quad (\text{S48})$$

The \mathbb{Z}_2 invariant $\nu(k_x, k_y)$ associated with a line node is obtained to be $\nu(k_x, k_y) = 1$ [$\nu(k_x, k_y) = 0$] within (out of) the line node. Therefore, $\nu_{i\eta} = 1$ when the four time-reversal invariant momenta on the $k_i = \eta\pi$ plane are enclosed by an odd number of line nodes, otherwise $\nu_{i\eta} = 0$. For instance, in the case that there is a single line node around $\Gamma_{\text{line}} = (\Gamma_{\text{line}}^x, \Gamma_{\text{line}}^y, \Gamma_{\text{line}}^z)$, the topological invariants are obtained to be

$$(\nu_1, \nu_2) = (\Gamma_{\text{line}}^x, \Gamma_{\text{line}}^y) / \pi, \quad \nu_0 = 1. \quad (\text{S49})$$

For the case of CaAgX, because a single line node appears around the Γ point, one gets

$$(\nu_1, \nu_2) = (0, 0), \quad \nu_0 = 1. \quad (\text{S50})$$

And also, one can calculate ν_3 in a similar manner since an additional mirror-reflection symmetry with respect to the xz plane is satisfied and the system has an energy gap and no integral pass along the k_y direction through the line node on the $k_z = \pi$ plane in the absence of spin-orbit interaction, In consequence, we obtain

$$\nu_{31} = 0. \quad (\text{S51})$$

The resultant \mathbb{Z}_2 invariant is given by 1;000.

S 4. 27-orbital model

Here we show bulk and surface electronic states of a tight-binding model for CaAgX which consists of the 27 orbitals, i.e., d orbitals of Ca, s orbitals of Ag, and p orbitals of X. Similarly to the 12-orbital model as discussed in the main context, spin-orbit interaction of CaAgP is neglected.

In CaAgAs, on the other hand, spin-orbit interaction only for the p orbitals of As atoms is taken into account in the form

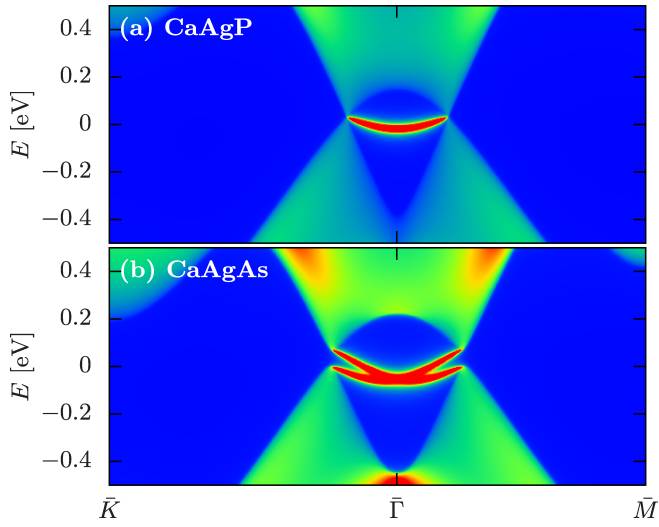


Fig. S 3. Angle-resolved density of states obtained by using the 27-orbital tight-binding model on the (0001) surface with the Ca_3X termination for $X = \text{P}$ (a), As (b).

of $H_{\text{SOI}} = \lambda \mathbf{L} \cdot \mathbf{S}$ with $\lambda = 0.07$ eV. The bulk and surface electronic states are shown in Figs. S 2 and S 3, respectively. The obtained energy bands for both CaAgP [Fig. S 2(a)] and CaAgAs [Fig. S 2(b)] well coincide with the first-principles bands not only in the low-energy regime ($E \sim 0$ eV) but also in high-energy regime ($E \sim 1$ eV). The electronic states for CaAgX on the (0001) surface with Ca_3X termination are shown in Fig. S 3, which are qualitatively the same as those of the 12-orbital models shown in Figs. 2(a) and 3(a). One can confirm that the model dependence of electronic states is negligibly small.